JACS
JOURNAL OF THE AMERICAN CHEMICAL SOCIETY
pubs.acs.org/JACS
Article

Giant Exciton Binding Energy in a Three-Dimensional Organic–Inorganic Hybrid Semiconductor

Rui Mei, Yi-Zhou Wang, Xue-Lu Liu, Thomas A. Schmedake, Yong Zhang,* and Ping-Heng Tan*

Cite This: J. Am. Chem. Soc. 2025, 147, 42867–42873
Read Online
ACCESS | Metrics & More | Article Recommendations

ABSTRACT: In a conventional three-dimensional (3D) semiconductor, exciton binding is significantly weaker than that of a low-dimensional system due to the absence of geometry confinement and strong dielectric screening. β-ZnTe(en)$_{0.5}$, a 3D II–VI organic–inorganic hybrid semiconductor, with subnanometer inorganic sheets, is predicted to possess an exceptionally large exciton binding energy, orders-of-magnitude higher than that of bulk ZnTe. However, experimental validation of this prediction is elusive. This study provides the first experimental confirmation of a large E_b in β-ZnTe(en)$_{0.5}$ using one-photon photoluminescence to detect the exciton ground state (1s) and two-photon photoluminescence excitation spectroscopy to probe the 2p-like exciton excited state. The 1s–2p separation can be taken as the lower-bound value of E_b and further used for estimating E_b by applying a hydrogenic model. The results reveal a 1s–2p separation of 280 meV at 300 K, which yields E_b exceeding 315 meV based on a hydrogenic model, the largest among 3D structures. The large E_b in β-ZnTe(en)$_{0.5}$ is derived from its 2D-like electronic properties. This work experimentally confirms the giant E_b in β-ZnTe(en)$_{0.5}$ together with the information on the exciton excited states, thereby setting a critical benchmark for more rigorous theoretical studies and establishing a novel spectroscopic approach for investigating a large group of hybrid semiconductors.

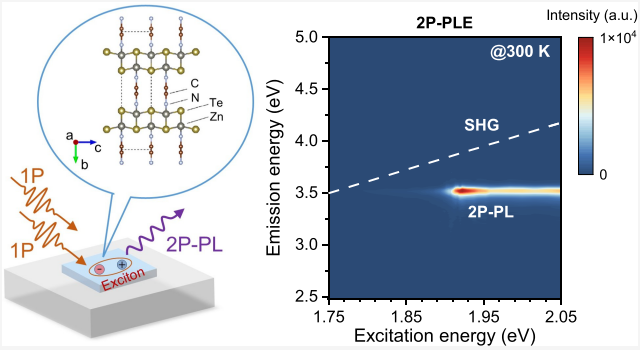

INTRODUCTION

Exciton plays a pivotal role in semiconductors as fundamental quasi-particles governing optical absorption, emission, and energy transfer, enabling advancements in photovoltaics, light-emitting devices, and quantum technologies.[1] In conventional three-dimensional (3D) semiconductor systems, excitonic effects are relatively weak. For example, in bulk GaAs and ZnTe, the exciton binding energies (E_b) are only 4.2 and 13 meV at low temperatures,[2,3] respectively. Such weak excitonic binding severely limits their application prospects in advanced optoelectronic devices where robust exciton stability is essential, particularly for room-temperature operation and quantum coherent manipulation. In low-dimensional semiconductor systems, the Coulomb interaction between electrons and holes can be significantly enhanced due to the quantum confinement effect and reduced dielectric screening, leading to pronounced excitonic effects and enhanced tunability.[1,4−7] The first approach to enhance the excitonic effect is using superlattices and quantum wells of inorganic semiconductors, e.g., GaAs/AlGaAs. It offers advantages in controlling the active volume through tailoring the well and barrier thicknesses and structural robustness as covalently bonded 3D structures, but the enhancement in the exciton binding energy is modest.[8] However, in one-dimensional (1D) carbon nanotubes, E_b reaches 300–400 meV, exhibiting strong dependence on tube diameter and chirality.[4,5] Similarly, in few-layer transition metal dichalcogenides (TMDs), a class of two-dimensional (2D) semiconductors, E_b ranges from 300 to 700 meV, which are nearly one to 2 orders of magnitude larger than those in 3D systems, underscoring the dominant role of excitons in their optoelectronic properties.[1,6,7]

β-ZnTe(en)$_{0.5}$ (en = $C_2N_2H_8$, ethylenediamine), a special 3D II–VI organic–inorganic hybrid semiconductor, with two monolayer thick ZnTe sheets, is expected to possess a strong excitonic effect with theoretical predictions suggesting an exceptionally large E_b (>200 meV),[9] which is even comparable to that of typical low-dimensional semiconductor systems, e.g., TMDs.[1] This level of E_b represents the largest known within 3D semiconductors. The pronounced excitonic effect in β-ZnTe(en)$_{0.5}$ offers significant advantages for developing ultralow-threshold coherent light sources and energy-efficient integrated exciton devices operating at room temperature, as it

Received: September 4, 2025
Revised: October 11, 2025
Accepted: October 31, 2025
Published: November 7, 2025

https://doi.org/10.1021/jacs.5c15468
J. Am. Chem. Soc. 2025, 147, 42867–42873

not only enhances exciton stability but also provides an ideal platform for exciton-polariton research.[10−12] Notably, the experimental determination of E_b for β-ZnTe(en)$_{0.5}$ remains challenging. The most straightforward method for estimating E_b in bulk semiconductors or conventional semiconductor quantum wells is to identify the ns (n = 1, 2, 3···) excitonic states in the linear absorption at low temperature, extrapolate them to get the band gap (E_g), and then determine E_b through $E_g = E_{1s} + E_b$.[1,3] However, previous linear absorption studies were not able to determine the E_g, due to the complexity of the band structure, as well as some practical difficulties working in the deep-ultraviolet spectral range.[9,13,14] Accurate experimental determination of E_b is essential for understanding the excitonic behavior of β-ZnTe(en)$_{0.5}$, a prototype of a large group of similar structures, making it urgent and important to find advanced spectroscopy techniques for experimental measurements.

This work reports an experimental study of the exciton excited state and E_b of β-ZnTe(en)$_{0.5}$ through combining one-photon photoluminescence (1P−PL) and two-photon photoluminescence excitation (2P−PLE) spectroscopy, which circumvents the difficulties encountered in the previous works. Owing to distinct selection rules for one-photon and two-photon transitions, the linear optical method 1P−PL can reveal the exciton ground state (1s), while 2P−PLE can be utilized to probe the exciton excited state, e.g., 2p. Since the energy difference between the 1s and 2p is closely related to the E_b, the corresponding 1s−2p separation can be used as a lower-bound estimate of E_b or to estimate the E_b based on a hydrogenic model. According to a 2D hydrogenic model, our results confirm an extraordinarily large E_b in β-ZnTe(en)$_{0.5}$ exceeding 315 meV at 300 K. The exceptionally large E_b in this 3D hybrid structure is derived from its 2D-like electronic properties. The experimental determination of E_b in β-ZnTe(en)$_{0.5}$ is critical for understanding the excitonic behavior in such an organic−inorganic hybrid semiconductor, providing essential insights for optimizing its optoelectronic performance.

RESULTS AND DISCUSSION

Organic−inorganic hybrid semiconductors have attracted considerable attention in recent years due to their outstanding optoelectronic properties and versatile applications.[15−18] One of the most extensively and intensively studied hybrid materials is the hybrid halide perovskite, which exhibits extraordinary application potentials in a wide range of applications, including photovoltaics and solid-state lighting.[13,19−22] Although the hybrid systems are of great interest for offering novel and enhanced properties, there are two typical drawbacks that restrict their practical application: poor long-term stability and structural disorder.[9,13,14] Thus, hybrid semiconductors with high crystallinity and long-term stability are highly appreciated. β-ZnTe(en)$_{0.5}$ (en = $C_2N_2H_8$, ethylenediamine) presents one of the very rare cases that exhibit these two characteristics simultaneously.[9,13,14,23]

β-ZnTe(en)$_{0.5}$ effectively addresses the aforementioned limitations. On the one hand, β-ZnTe(en)$_{0.5}$ demonstrates exceptional long-term stability, with a shelf life exceeding 15 years.[13] On the other hand, this hybrid semiconductor is a perfectly ordered structure, representing an ideal hybrid semiconductor with both long- and short-range order.[14] Its crystallinity has been reported to rival that of high-quality elemental and binary semiconductors.[13,23,24] The structural unit of β-ZnTe(en)$_{0.5}$ consists of two-monolayer-thick ZnTe(110) slabs interconnected by ethylenediamine molecules forming covalent-like bonding through Zn and N atoms, as shown in Figure 1(a). β-ZnTe(en)$_{0.5}$ crystal can be regarded

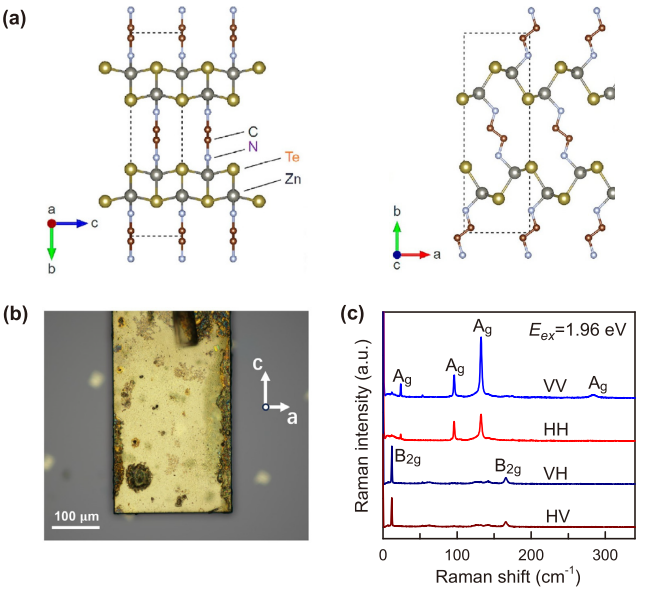

Figure 1. (a) Structure of β-ZnTe(en)$_{0.5}$. (b) Optical image of β-ZnTe(en)$_{0.5}$. (c) Raman spectra of β-ZnTe(en)$_{0.5}$ obtained under different excitation polarization configurations.

as a perfect 1D superlattice, distinct from conventional 1D inorganic superlattices, such as GaAs/AlGaAs,[8] which typically suffer from interfacial lattice mismatch and alloying effects at the interfaces. It is an orthorhombic crystal with space group $Pnnm$, point group D_{2h}, and stacking axis b and in-plane axes a and c.[23,24] Figure 1(b) shows the optical image of the β-ZnTe(en)$_{0.5}$ flake, with the marked in-plane axes a and c. Notably, β-ZnTe(en)$_{0.5}$ exhibits strong in-plane anisotropy, where the absorption coefficient along the c-axis is significantly larger than that along the a-axis.[9,14] Because of the in-plane anisotropy, the crystalline orientation was fixed in subsequent experiments with the vertical (V) and horizontal (H) directions in the excitation (or emission) polarization directions aligned parallel to the c-axis and a-axis, respectively.

To investigate the intrinsic properties of β-ZnTe(en)$_{0.5}$, Raman spectroscopy is utilized to verify that the sample exhibits a pristine structure. As shown in Figure 1(b), there are some rough areas concentrated at the edges of the sample, which might be caused by the residues left over from the sample synthesis process. In this study, we first identified a clean and uniform area and then examined it by Raman spectroscopy to make sure that the material yielded Raman features of the pristine structure. The Raman spectra shown in Figure 1(c) were obtained from a uniform and flat area on the sample under different excitation polarization configurations. The corresponding Raman spectra exhibit multiple sharp peaks similar to those reported previously.[13,25] Their symmetry assignments have been reported according to DFT calculations of phonon modes and their Raman tensors.[13] The sharp Raman peaks indicate a high degree of structural ordering in the hybrid semiconductor, e.g., the full width at half-maximum of the strongest mode at 133.2 cm^{-1} is only 2.4 cm^{-1}. In addition, the β-ZnTe(en)$_{0.5}$ sample used in this study does not

https://doi.org/10.1021/jacs.5c15468
J. Am. Chem. Soc. 2025, 147, 42867−42873

show degradation because no degradation-related Te peaks can be found in the corresponding Raman spectra, which would appear at 122 and 141 cm^{-1}.[13] After confirmation that the sample exhibited a high crystal quality, the 1P−PL and 2P−PLE spectra were taken from the identified areas.

Although the exciton ground state is readily observable in optical absorption and other spectroscopy measurements for a material with decent crystallinity, it is nontrivial to identify the quasiparticle band gap E_g using a spectroscopy technique. For instance, linear reflectance does not usually show a well-defined feature at the quasiparticle band gap, and photoreflectance (a modulated reflectance) also only yields a feature near the excitonic band gap, as in the case for a carefully studied prototype system GaAs.[26] As mentioned above, the most straightforward method for estimating E_b in bulk semiconductors or conventional semiconductor quantum wells is to identify the ns (n = 1, 2, 3⋯) excitonic states in the linear absorption at low temperature, extrapolate them to get E_g, then determine E_b through $E_g = E_{1s} + E_b$. However, previous linear absorption studies on β-ZnTe(en)$_{0.5}$ failed to yield clearly identifiable ns exciton excited states or the E_g,[9,13,14] due to the inherent complexity of the band structure, compounded by practical challenges associated with measurements in the deep-ultraviolet spectral range. Here, an alternative approach is to probe the exciton excited states using 2P−PLE and evaluate E_b from the level spacing based on a theoretical model. In the simple 2D hydrogenic model, electron−hole pairs can form a series of exciton Rydberg-like states (E_n), with $E_n = -E_b/[4(n - 1/2)^2]$.[1,6,27,28] Each state n (= 1, 2, 3⋯) is degenerate with angular momentum l = 0, ± 1,⋯, ± (n − 1). According to the 2D hydrogenic model, the energy separations between the excited states and ground state account for specific fractions of E_b. For example, the energy separation between the 2p state (n = 2, l = ±1) and the 1s state (n = 1, l = 0) is 8/9 of E_b.[27,28] Thus, accurately measuring the energies of both the ground state and an excited state (e.g., 2p) allows the determination of E_b in the 2D hydrogenic model.

Here, 1P−PL is adopted to obtain the energy of the exciton ground state (E_{1s}) of β-ZnTe(en)$_{0.5}$ at room temperature.[9,13] Figure 2(a) presents the 1P−PL spectra of β-ZnTe(en)$_{0.5}$ excited by 4.28 eV under different excitation polarization configurations at 300 K. A prominent PL peak is observed at

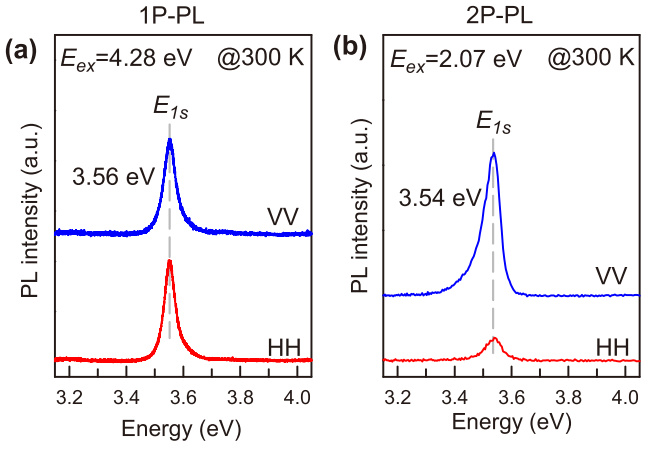

Figure 2. (a) 1P−PL spectra of β-ZnTe(en)$_{0.5}$ obtained under different excitation polarization configurations at 300 K. (b) 2P−PL spectra of β-ZnTe(en)$_{0.5}$ obtained under different excitation polarization configurations at 300 K.

3.56 eV, which directly provides the experimental value of E_{1s}. Notably, the emission signals in the 1P−PL spectra under both VV and HH configurations do not exhibit significant anisotropy.[9] As for the detection of exciton excited states, nonlinear optical effects, such as two-photon photoluminescence (2P−PL), can play a crucial role. In the 2P−PL process, the electron in the valence band undergoes a two-photon absorption transition to an exciton excited state, followed by an ultrafast relaxation process to the exciton ground state, and finally a one-photon interband radiative transition.[7] Figure 2(b) demonstrates the PL spectra of β-ZnTe(en)$_{0.5}$ excited by 2.07 eV pulses, in which a significant 2P−PL signal can be observed. Although the observed 2P−PL signal (also marked E_{1s}) is related to the 1s state, it exhibits distinct spectral characteristics in comparison with the E_{1s} peak in 1P−PL spectrum, including a slight red shift of peak position, significant changes in the spectral line shape, and more pronounced anisotropy. The corresponding changes can be attributed to the fact that the excitation wavelength of the 2P−PL spectra falls within the visible range, allowing for the generation of luminescence signals from deeper regions of the sample. The self-absorption effect, which occurs as the emission signal propagates from the deeper region to the surface, results in a noticeable red shift in the peak position and asymmetry in the spectral shape.[29] The intensity of the 2P−PL emission signal under VV configuration is much stronger than that under HH configuration. The enhanced anisotropy is due to the different selection rules in the one-photon and two-photon excitations.[30]

According to the interband dipole transition theory, the transition process must simultaneously satisfy energy conservation and symmetry selection rules. The latter depends on the symmetry of the final state: one-photon transitions are only allowed to exciton states with even parity, e.g., 1s/2s state, while two-photon transitions can access exciton states with odd parity, e.g., 2p state.[1,4−7,27,28,31] Based on the corresponding selection rules, one can obtain a complete 2P−PLE spectrum by tuning E_{ex} and probe the exciton excited states according to the two-photon resonant absorption, particularly the first allowed excited state, i.e., 2p state, as shown in Figure 3(a). The contour plot Figure 3(b) shows the measured PL spectra of β-ZnTe(en)$_{0.5}$ with different E_{ex} values under the VV configuration at 300 K. As the E_{ex} values gradually increase, a typical 2P−PL signal emerges, characterized by its E_{ex}-independent emission peak position, and exhibits resonant enhancement at specific E_{ex}. In principle, second-harmonic generation (SHG) can also be employed to probe excitonic excited states.[7] However, this approach is not applicable to β-ZnTe(en)$_{0.5}$ due to its centrosymmetric crystal structure,[13,23] which directly results in the absence of SHG signals, as indicated by the white dashed line for the would-be SHG emission energy in Figure 3(b).

The 2P−PLE profile of β-ZnTe(en)$_{0.5}$ can be obtained as a horizontal cut in the contour plot of Figure 3(b), taken at the energy corresponding to E_{1s}, as shown in Figure 3(c). The excitation profile demonstrates that the 2P−PL signal is absent under low E_{ex}, especially when $E_{ex} = 1.78$ eV $\left(= \frac{1}{2}E_{1s}\right)$. However, a significant enhancement of the 2P−PL signal is observed at $E_{ex} = 1.92$ eV. The corresponding peak position in the 2P−PLE profile can be identified as one-half of the 2p state energy $\left(\frac{1}{2}E_{2p}\right)$, the lowest-lying symmetry-allowed state for the

https://doi.org/10.1021/jacs.5c15468
J. Am. Chem. Soc. 2025, 147, 42867−42873

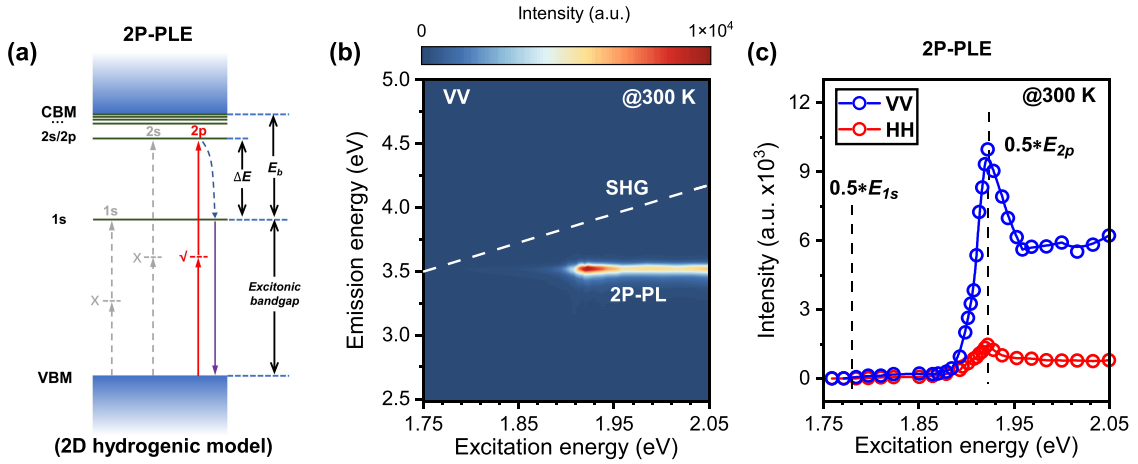

Figure 3. (a) Schematic of detecting E_b by 2P−PLE. (b) Contour plot of 2P−PLE spectra of β-ZnTe(en)$_{0.5}$ obtained by tuning E_{ex} under VV configuration at 300 K. The white dashed line indicates the position of the 2 × E_{ex}, which is also the theoretical position of the would-be SHG signal. When scanning E_{ex}, the SHG signal is always absent in β-ZnTe(en)$_{0.5}$. (c) 2P−PLE spectra of β-ZnTe(en)$_{0.5}$ under VV and HH configurations at 300 K.

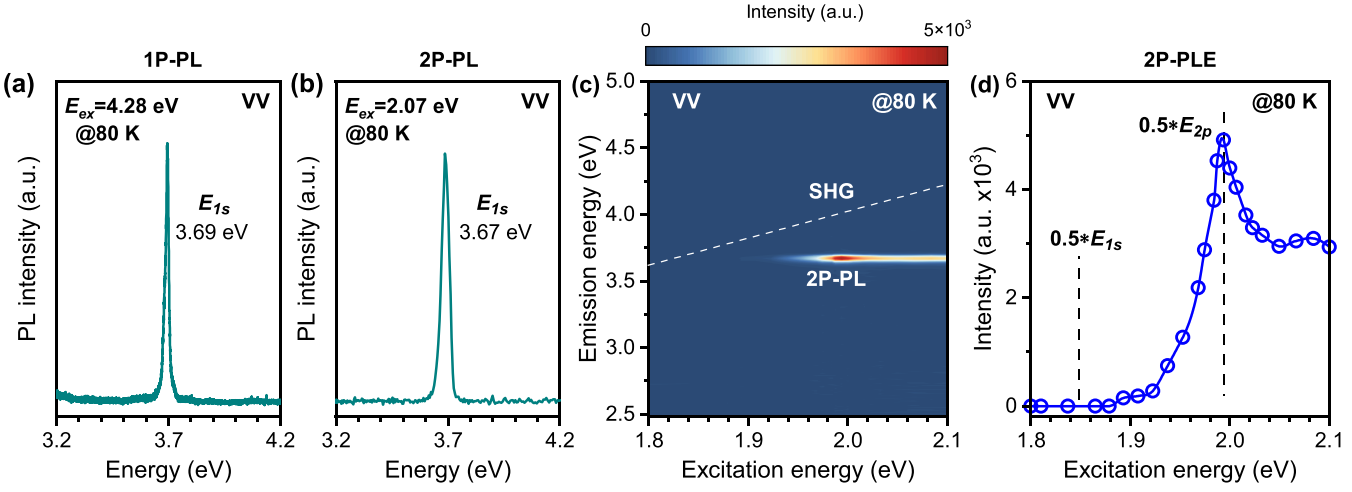

Figure 4. (a) 1P−PL of β-ZnTe(en)$_{0.5}$ excited by 4.28 eV under the VV configuration at 80 K. (b) 2P−PL of β-ZnTe(en)$_{0.5}$ excited by 2.07 eV under the VV configuration at 80 K. (c) Contour plot of 2P−PLE spectra of β-ZnTe(en)$_{0.5}$ obtained by tuning E_{ex} under the VV configuration at 80 K. (d) 2P−PLE profile of β-ZnTe(en)$_{0.5}$ under the VV configuration at 80 K.

two-photon transition. Based on the above observation, the energy difference between the 1*s* and 2*p* states can be obtained: $\Delta E = E_{2p} - E_{1s} = 280$ meV. Combining the determined ΔE with the position of the 2*p* state relative to the continuum in the 2D hydrogenic model,[27,28] one can estimate an overall E_b of β-ZnTe(en)$_{0.5}$: $E_b = \frac{9}{8}\Delta E = 315$ meV. Owing to the pronounced in-plane anisotropy of β-ZnTe(en)$_{0.5}$ along the *a*-axis and *c*-axis, we further explored its exciton properties by measuring the corresponding 2P−PLE profiles under the HH configuration through tuning E_{ex}, as presented in Figure 3(c). Compared with the one obtained under VV configuration, the 2P−PLE profile under the HH configuration exhibits similar features, including a similar excitation profile and an identical resonance absorption peak position. Their primary distinction lies in the intensity, which shows significant anisotropy due to the difference in the two-photon absorption coefficient along the *a*-axis and *c*-axis of the crystal. Consequently, the E_b of β-ZnTe(en)$_{0.5}$ can also be estimated based on the experimental results obtained under the HH configuration, which is consistent with the value derived from the VV configuration. Notably, in the corresponding 2P−PLE measurements, there is no resonance signature associated with the band edge, even when the two-photon excitation energy reaches ∼630 meV above the 1*s* state. The fundamental reason is that there is no expected singularity in the density of states at the quasiparticle band gap to give rise to a unique optical signature.

Low-temperature experimental conditions offer several advantages, such as narrower emission line widths and enhanced ability to resolve spectral features. Thus, performing 1P−PL and 2P−PLE experiments at low temperatures is expected to yield higher precision data and offer robust validation for room-temperature results. Figure 4(a,b) shows the 1P−PL and 2P−PL of β-ZnTe(en)$_{0.5}$ observed under VV configuration at 80 K. In comparison with the room temperature results, both the 1P−PL and 2P−PL signals at 80 K exhibit narrower line widths, which facilitates a more accurate determination of E_{1s}. Due to the persistent influence of the self-absorption effect on the 2P−PL signal, the E_{1s} (3.69 eV) obtained from 1P−PL is adopted as the experimental value of the 1*s* state. Through tuning of the E_{ex} at 80 K, a

https://doi.org/10.1021/jacs.5c15468
J. Am. Chem. Soc. 2025, 147, 42867−42873

complete 2P−PLE spectrum can be probed, as shown in Figure 4(c). The intensity of the 2P−PL signal with narrow line width also exhibits an E_{ex}-dependent feature, similar to the characteristic observed at room temperature. Figure 4(d) directly illustrates the 2P−PLE profile at 80 K. E_{2p} can be estimated based on the position of the resonance peak in the 2P−PLE profile. Combined with the experimentally determined E_{1s}, the $1s-2p$ separation at 80 K can be calculated: $\Delta E = E_{2p} - E_{1s} = 290$ meV. Similarly, based on the 2D hydrogenic model, the E_b at 80 K is determined to be 326 meV, slightly higher than the room-temperature value (by 10 meV or 3.5%). The small difference could be related to the temperature dependence of the electronic band structure and the associated change in the dielectric constants. For instance, in GaAs, the refractive index increases slightly with temperature, which contributes partially to the slight reduction in the E_b between the very low temperature and 300 K.[32] The subtle temperature effect of the hybrid requires further studies.

The strong excitonic binding of the corresponding 3D β-ZnTe(en)$_{0.5}$ derives from its excellent artificial superlattice structure, where the molecule serves as electronic confinement barriers and dielectric screening modulators that reduce Coulomb interaction screening.[9,13] This structural characteristic endows the corresponding 3D hybrid system with key electronic properties of a 2D system, including the strong quantum confinement of both electrons and holes to the inorganic region and strong exciton effect.[9,33] By synergistically combining electronic confinement and dielectric screening modulation, β-ZnTe(en)$_{0.5}$ achieves orders-of-magnitude higher E_b than inorganic ZnTe, in a 3D framework.[9] Its E_b is even comparable to those found in low-dimensional semiconductors, e.g., atomically thin TMDs, or 1D carbon nanotubes. Moreover, although conventional 3D semiconductors tend to exhibit a positive correlation between the E_b and E_g,[34] β-ZnTe(en)$_{0.5}$ has a much larger E_b than those with even much larger E_g, such as diamond (E_b = 80 meV/E_g = 5.5 eV)[35] and AlN (E_b = 57 meV/E_g = 6.1 eV).[36] This feature indicates that the wide band gap is not the key factor for the large E_b of β-ZnTe(en)$_{0.5}$.

The corresponding experimental verification of a large E_b in β-ZnTe(en)$_{0.5}$ holds significant importance. The exciton in β-ZnTe(en)$_{0.5}$ should be viewed as a 2D-like Wannier−Mott exciton, similarly to the cases of those monolayer TMDs, rather than a Frenkel exciton, because the electronic wave functions on the inorganic sheets are extended with dispersions similar to those of bulk ZnTe.[9] This character makes the giant E_b value much more remarkable. Beyond this, it demonstrates that the organic−inorganic hybrid strategy can profoundly enhance the E_b of a 3D narrow-band gap semiconductor. The degree of enhancement achieved here is difficult to realize in conventional inorganic semiconductors through typical quantum confinement approaches. For example, only a modest enhancement in E_b can be achieved in an inorganic superlattice like GaAs/AlGaAs.[8] For the past two decades, planar quantum wells, e.g., GaAs multiple quantum wells, have been utilized for universal polaritonic platforms for generating polariton condensates.[37,38] However, their relatively small E_b values necessitate extremely low operating temperatures for exciton devices. To develop ultralow-threshold coherent light sources and energy-efficient integrated polaritonic devices operating at room temperature, it is pivotal to explore room-temperature exciton devices and polariton condensate devices.[12] Based on our experimental investigation, due to the large E_b of β-ZnTe(en)$_{0.5}$ against thermal fluctuation, the corresponding organic−inorganic hybrid 3D semiconductor is a very attractive candidate for these applications.

Finally, it is necessary to discuss the limitations of the 2D hydrogenic model in estimating the E_b of β-ZnTe(en)$_{0.5}$. We are aware that neither the 3D nor 2D hydrogenic model can accurately describe its excitonic states. Comparatively, the 2D hydrogenic model likely can offer a better estimate for the E_b than the 3D model due to the highly confined nature of the band edge state wave functions along the organic−inorganic stacking direction. The ideal 2D model assumes (1) isotropic in-plane electronic dispersion, (2) a single pair of the conduction and valence bands, and (3) a uniform in-plane dielectric environment and no dielectric screening along the out-of-plane direction. The complexity in the band structure and strong anisotropy in electronic dispersion and dielectric response of this biaxial crystal β-ZnTe(en)$_{0.5}$ make the hydrogenic model obviously an overly simplified one.[9] The relatively large line width in the 2P−PLE profile, particularly nearly independent of the temperature, suggests that the supposed "$2p$" peak could include the contributions of various excited states as a result of the complex excitonic energy spectrum. The complexity could result in an elevated E_{1s}.[6,27] Consequently, the actual $1s-2p$ separation ΔE accounts for a smaller fraction of E_b than that in the ideal case, i.e., $\Delta E/E_b < 8/9$. The large E_b indicates that the exciton wave function includes the contributions from a large region of the $\boldsymbol{k}$ space in the Brillouin zone,[9] which can lead to a more complex exciton spectrum than that of a hydrogenic model. Ideally, one should perform a rigorous theoretical modeling by solving a GW-based Bethe−Salpeter equation to obtain the excitonic spectrum of the hybrid, as has been done for monolayer TMDs,[6] and to interpret the two-photon absorption results, then extrapolate the quasiparticle band gap. Unfortunately, because of the much larger unit cell of the hybrid semiconductor (32 atoms/unit cell), the calculation is very challenging even with the most advanced computational approach.[39]

Given that the primary motivation of this investigation is to validate that the hybrid structure indeed exhibits a large E_b against thermal fluctuation at room temperature for its potential room-temperature applications, a conservative assessment is to take the experimentally measured $1s-2p$ separation (280 meV at 300 K or 290 meV at 80 K) as a lower-bound value of E_b without invoking any specific model. Nevertheless, applying a hydrogen model could give a semiquantitative estimate for the actual E_b. The discrepancy between the estimated E_b values by the 2D and 3D hydrogenic model could be roughly viewed as the uncertainty range. To achieve a more accurate determination of E_b, further theoretical studies based on our experimental results are required in the future.

CONCLUSIONS

In conclusion, this work has experimentally probed the exciton ground state ($1s$) and excited state ($2p$) in β-ZnTe(en)$_{0.5}$ by complementary linear and nonlinear optical methods. The experimental results reveal a $1s-2p$ separation of 280 meV (290 meV) at 300 K (80 K), which represents a major contribution to E_b, strongly supporting the prediction of a strong exciton effect in the corresponding hybrid semiconductor. One can directly take the corresponding $1s-2p$ separation as an estimation of E_b, or estimate the E_b based on the hydrogenic model. Applying the 2D hydrogenic model

https://doi.org/10.1021/jacs.5c15468
J. Am. Chem. Soc. 2025, 147, 42867−42873

yields E_b = 315 (326) meV at 300 K (80 K). Despite the oversimplification nature of the 2D hydrogenic model, it is reasonable to conclude that the E_b in this hybrid structure exceeds 300 meV. The strong excitonic binding in 3D β-ZnTe(en)$_{0.5}$ originates from the synergistic effect of electronic confinement and dielectric screening modulation. The corresponding E_b ranks among the highest reported levels for known 3D semiconductors, rivaling those of typical 2D systems. The experimental determination of E_b in β-ZnTe(en)$_{0.5}$ not only contributes to a deeper comprehension of excitonic behavior in such an organic−inorganic hybrid semiconductor but also offers critical insights for advancing theoretical investigations. This work lays the ground for the next step to explore the exciton-polariton properties at room temperature for quantum informatics-related applications.

EXPERIMENTAL SECTION

The samples of β-ZnTe(en)$_{0.5}$ were synthesized following reported literature procedures.[13,23] Raman spectra were measured under a backscattering configuration at 300 K with a JobinYvon HR800 Raman system equipped with 1800 grooves/mm gratings, coupled with a liquid-nitrogen-cooled charge-coupled device (CCD) and a 100× objective (numerical aperture = 0.90). The E_{ex} was 1.96 eV from a He−Ne laser. After the intrinsic and uniform β-ZnTe(en)$_{0.5}$ sample area was identified using Raman spectroscopy, the measurement location was fixed to avoid any influence caused by the roughness at the sample edges. The 1P−PL and 2P−PL were obtained using a SmartRaman confocal micro-Raman module (Institute of Semiconductors, Chinese Academy of Sciences) coupled with a Horiba iHR550 spectrometer. This PL system is equipped with an air-cooled CCD and two gratings with groove densities of 1800 and 100 grooves/mm. A 74× reflective objective lens was used to collect the emission signal. A fs-Ti:sapphire Laser operating at an 80 MHz repetition rate was used to provide the required excitation pulses. The 2P−PL spectra at 80 K were also measured in a liquid-nitrogen-cooled cryostat (Janis ST-500).

ASSOCIATED CONTENT

Data Availability Statement

The data that support the findings of this study are available from the corresponding author upon reasonable request.

AUTHOR INFORMATION

Corresponding Authors

Yong Zhang − *Department of Electrical and Computer Engineering, University of North Carolina at Charlotte, Charlotte, North Carolina 28223, United States;* orcid.org/0000-0003-4781-1583; Email: yong.zhang@uncc.edu

Ping-Heng Tan − *State Key Laboratory of Semiconductor Physics and Chip Technologies, Institute of Semiconductors, Chinese Academy of Sciences, Beijing 100083, China; Center of Materials Science and Optoelectronics Engineering, University of Chinese Academy of Sciences, Beijing 100049, China;* orcid.org/0000-0001-6575-1516; Email: phtan@semi.ac.cn

Authors

Rui Mei − *State Key Laboratory of Semiconductor Physics and Chip Technologies, Institute of Semiconductors, Chinese Academy of Sciences, Beijing 100083, China; Center of Materials Science and Optoelectronics Engineering, University of Chinese Academy of Sciences, Beijing 100049, China;* orcid.org/0009-0005-5684-5306

Yi-Zhou Wang − *Department of Chemistry, University of North Carolina at Charlotte, Charlotte, North Carolina 28223, United States*

Xue-Lu Liu − *State Key Laboratory of Semiconductor Physics and Chip Technologies, Institute of Semiconductors, Chinese Academy of Sciences, Beijing 100083, China;* orcid.org/0000-0001-9156-6760

Thomas A. Schmedake − *Department of Chemistry, University of North Carolina at Charlotte, Charlotte, North Carolina 28223, United States*

Complete contact information is available at: https://pubs.acs.org/10.1021/jacs.5c15468

Notes

The authors declare no competing financial interest.

ACKNOWLEDGMENTS

We acknowledge the support from the National Key Research and Development Program of China (Grant No. 2023YFA1407000), the Strategic Priority Research Program of CAS (Grant No. XDB0460000), the National Natural Science Foundation of China (Grant Nos. 12127807 and 12393832), and the ARO/Complex Dynamics and Systems Program under Grant No. W911NF-23-1-0215 at UNC Charlotte.

REFERENCES

(1) Wang, G.; Chernikov, A.; Glazov, M. M.; Heinz, T. F.; Marie, X.; Amand, T.; Urbaszek, B. Colloquium: Excitons in Atomically Thin Transition Metal Dichalcogenides. *Rev. Mod. Phys.* **2018**, *90*, No. 021001.

(2) Venghaus, H.; Dean, P. J. Shallow-Acceptor, Donor, Free-Exciton, and Bound-Exciton States in High-Purity Zinc Telluride. *Phys. Rev. B* **1980**, *21*, 1596−1609.

(3) Weisbuch, C.; Benisty, H.; Houdre, R. Overview of Fundamentals and Applications of Electrons, Excitons and Photons in Confined Structures. *J. Lumin.* **2000**, *85*, 271−293.

(4) Wang, F.; Dukovic, G.; Brus, L. E.; Heinz, T. F. The Optical Resonances in Carbon Nanotubes Arise from Excitons. *Science* **2005**, *308*, 838−841.

(5) Maultzsch, J.; Pomraenke, R.; Reich, S.; Chang, E.; Prezzi, D.; Ruini, A.; Molinari, E.; Strano, M. S.; Thomsen, C.; Lienau, C. Exciton Binding Energies in Carbon Nanotubes from Two-Photon Photoluminescence. *Phys. Rev. B* **2005**, *72*, No. 241402.

(6) Ye, Z.; Cao, T.; O'Brien, K.; Zhu, H.; Yin, X.; Wang, Y.; Louie, S. G.; Zhang, X. Probing Excitonic Dark States in Single-Layer Tungsten Disulphide. *Nature* **2014**, *513*, 214−218.

(7) Wang, G.; Marie, X.; Gerber, I.; Amand, T.; Lagarde, D.; Bouet, L.; Vidal, M.; Balocchi, A.; Urbaszek, B. Giant Enhancement of the Optical Second-Harmonic Emission of WSe_2 Monolayers by Laser Excitation at Exciton Resonances. *Phys. Rev. Lett.* **2015**, *114*, No. 097403.

(8) Bajaj, K. Use of Excitons in Materials Characterization of Semiconductor System. *Mater. Sci. Eng.: R: Rep.* **2001**, *34*, 59−120.

(9) Zhang, Y.; Dalpian, G. M.; Fluegel, B.; Wei, S.-H.; Mascarenhas, A.; Huang, X.-Y.; Li, J.; Wang, L.-W. Novel Approach to Tuning the Physical Properties of Organic-Inorganic Hybrid Semiconductors. *Phys. Rev. Lett.* **2006**, *96*, No. 026405.

(10) Su, R.; Fieramosca, A.; Zhang, Q.; Nguyen, H. S.; Deleporte, E.; Chen, Z.; Sanvitto, D.; Liew, T. C. H.; Xiong, Q. Perovskite Semiconductors for Room-Temperature Exciton-Polaritonics. *Nat. Mater.* **2021**, *20*, 1315−1324.

(11) Masharin, M.; Samusev, A.; Bogdanov, A.; Iorsh, I.; Demir, H.; Makarov, S. Room-Temperature Exceptional-Point-Driven Polariton Lasing from Perovskite Metasurface. *Adv. Funct. Mater.* **2023**, *33*, No. 2215007.

(12) Song, J.; Ghosh, S.; Deng, X.; et al. Room-Temperature Continuous-Wave Pumped Exciton Polariton Condensation in a Perovskite Microcavity. *Sci. Adv.* **2025**, *11*, No. eadr1652.
(13) Ye, T.; Kocherga, M.; Sun, Y.-Y.; Nesmelov, A.; Zhang, F.; Oh, W.; Huang, X.-Y.; Li, J.; Beasock, D.; Jones, D. S.; Schmedake, T. A.; Zhang, Y. II-VI Organic-Inorganic Hybrid Nanostructures with Greatly Enhanced Optoelectronic Properties, Perfectly Ordered Structures, and Shelf Stability of Over 15 Years. *ACS Nano* **2021**, *15*, 10565−10576.
(14) Zhang, Y. II-VI Based Organic-Inorganic Hybrid Structures: Brief Review and Perspective. *J. Lumin.* **2022**, *248*, No. 118936.
(15) Sanchez, C.; Julián, B.; Belleville, P.; Popall, M. Applications of Hybrid Organic-Inorganic Nanocomposites. *J. Mater. Chem.* **2005**, *15*, 3559−3592.
(16) Grätzel, M. The Light and Shade of Perovskite Solar Cells. *Nat. Mater.* **2014**, *13*, 838−842.
(17) Saparov, B.; Mitzi, D. B. Organic-Inorganic Perovskites: Structural Versatility for Functional Materials Design. *Chem. Rev.* **2016**, *116*, 4558−4596.
(18) Zhao, Y.; Zhu, K. Organic-Inorganic Hybrid Lead Halide Perovskites for Optoelectronic and Electronic Applications. *Chem. Soc. Rev.* **2016**, *45*, 655−689.
(19) Kojima, A.; Teshima, K.; Shirai, Y.; Miyasaka, T. Organometal Halide Perovskites as Visible-Light Sensitizers for Photovoltaic Cells. *J. Am. Chem. Soc.* **2009**, *131*, 6050−6051.
(20) Xing, J.; Liu, X. F.; Zhang, Q.; Ha, S. T.; Yuan, Y. W.; Shen, C.; Sum, T. C.; Xiong, Q. Vapor Phase Synthesis of Organometal Halide Perovskite Nanowires for Tunable Room-Temperature Nanolasers. *Nano Lett.* **2015**, *15*, 4571−4577.
(21) Zhang, Q.; Shang, Q.; Su, R.; Do, T. T. H.; Xiong, Q. Halide Perovskite Semiconductor Lasers: Materials, Cavity Design, and Low Threshold. *Nano Lett.* **2021**, *21*, 1903−1914.
(22) Shi, Y.; Deng, X.; Gan, Y.; Xu, L.; Zhang, Q.; Xiong, Q. Ten Years of Perovskite Lasers. *Adv. Mater.* **2025**, *37*, No. 2413559.
(23) Huang, X.; Li, J.; Zhang, Y.; Mascarenhas, A. From 1D Chain to 3D Network: Tuning Hybrid II-VI Nanostructures and Their Optical Properties. *J. Am. Chem. Soc.* **2003**, *125*, 7049−7055.
(24) Zhang, Y.; Islam, Z.; Ren, Y.; Parilla, P. A.; Ahrenkiel, S. P.; Lee, P. L.; Mascarenhas, A.; McNevin, M. J.; Naumov, I.; Fu, H.-X.; Huang, X.-Y.; Li, J. Zero Thermal Expansion in a Nanostructured Inorganic-Organic Hybrid Crystal. *Phys. Rev. Lett.* **2007**, *99*, No. 215901.
(25) Ye, T.; Sun, Y.-Y.; Kocherga, M.; Nesmelov, A.; Schmedake, T. A.; Zhang, Y. Degradation Kinetics of Organic−Inorganic Hybrid Materials from Micro-Raman Spectroscopy and Density-Functional Theory: The Case of β -ZnTe$(en)_{0.5}$. *Small* **2023**, *19*, No. 2302935.
(26) Zhang, Y. Optical Spectroscopy Methods for Determining Semiconductor Bandgaps. *Chin. J. Lumin.* **2025**, *46*, 1271−1282.
(27) He, K.; Kumar, N.; Zhao, L.; Wang, Z.; Mak, K. F.; Zhao, H.; Shan, J. Tightly Bound Excitons in Monolayer WSe_2. *Phys. Rev. Lett.* **2014**, *113*, No. 026803.
(28) Zhu, B.; Chen, X.; Cui, X. Exciton Binding Energy of Monolayer WS_2. *Sci. Rep.* **2015**, *5*, No. 9218.
(29) Mooradian, A.; Fan, H. Y. Recombination Emission in InSb. *Phys. Rev.* **1966**, *148*, 873−885.
(30) Rustagi, K. C.; Pradere, F.; Mysyrowicz, A. Two-Photon Absorption in Cu_2O. *Phys. Rev. B* **1973**, *8*, 2721−2732.
(31) Mahan, G. D. Theory of Two-Photon Spectroscopy in Solids. *Phys. Rev.* **1968**, *170*, 825−838.
(32) Madelung, O. *Semiconductors: Data Handbook*; Springer Berlin Heidelberg: Berlin, Heidelberg, 2004.
(33) Fluegel, B.; Zhang, Y.; Mascarenhas, A.; Huang, X.; Li, J. Electronic Properties of Hybrid Organic-Inorganic Semiconductors. *Phys. Rev. B* **2004**, *70*, No. 205308.
(34) Haug, H.; Koch, S. W. *Quantum Theory of the Optical and Electronic Properties of Semiconductors*; World Scientific: Singapore, 2009.
(35) Chen, Y.; Jin, P.; Zhou, G.; Feng, M.; Fu, F.; Wu, J.; Wang, Z. Investigation of Excitonic Recombination in Single-Crystal Diamond with Cathodoluminescence Spectroscopy. *J. Lumin.* **2020**, *226*, No. 117428.
(36) Yamada, Y.; Choi, K.; Shin, S.; Murotani, H.; Taguchi, T.; Okada, N.; Amano, H. Photoluminescence from Highly Excited AlN Epitaxial Layers. *Appl. Phys. Lett.* **2008**, *92*, No. 131912.
(37) Deng, H.; Weihs, G.; Santori, C.; Bloch, J.; Yamamoto, Y. Condensation of Semiconductor Microcavity Exciton Polaritons. *Science* **2002**, *298*, 199−202.
(38) Kasprzak, J.; Richard, M.; Kundermann, S.; Baas, A.; Jeambrun, P.; Keeling, J. M. J.; Marchetti, F. M.; Szymańska, M. H.; André, R.; Staehli, J. L.; Savona, V.; Littlewood, P. B.; Deveaud, B.; Dang, L. S. Bose−Einstein Condensation of Exciton Polaritons. *Nature* **2006**, *443*, 409−414.
(39) Jia, F.; Tang, Z.; Cruz, G. J.; Gao, W.; Xu, S.; Ren, W.; Zhang, P. Quasiparticle and Excitonic Structures of Few-Layer and Bulk GaSe: Interlayer Coupling, Self-Energy, and Electron-Hole Interaction. *Phys. Rev. Appl* **2024**, *21*, No. 054019.

https://doi.org/10.1021/jacs.5c15468
J. Am. Chem. Soc. 2025, 147, 42867−42873